Journal of Inorganic Biochemistry 183 (2018) 184–190

Contents lists available at ScienceDirect

Journal of Inorganic Biochemistry

journal homepage: www.elsevier.com/locate/jinorgbio

An optimized low-cost protocol for standardized production of iron-free apoferritin nanocages with high protein recovery and suitable conformation for nanotechnological applications

Italo Moglia[a], Margarita Santiago[b], Álvaro Olivera-Nappa[a,b,*], Mónica Soler[a,*]

[a] Department of Chemical Engineering, Biotechnology and Materials, FCFM, University of Chile, Beauchef 851, Santiago, Chile
[b] Center for Biotechnology and Bioengineering – CeBiB, FCFM, University of Chile, Beauchef 851, Santiago, Chile

ARTICLE INFO

Keywords:
Apoferritin production
Iron-devoided ferritin
Iron chelators
pH effect
Monomeric ferritin
Oligomeric ferritin

ABSTRACT

Ferritin is a globular protein that consists of 24 subunits forming a hollow nanocage structure that naturally stores iron oxyhydroxides. Elimination of iron atoms to obtain the empty protein called apoferritin is the first step to use this organic shell as a nanoreactor for different nanotechnological applications. Different protocols have been reported for apoferritin formation, but some are time consuming, others are difficult to reproduce and protein recovery yields are seldom reported. Here we tested several protocols and performed a complete material characterization of the apoferritin products using size exclusion chromatography, UV–vis spectroscopy, inductively coupled plasma optical emission spectrometry and dynamic light scattering. Our best method removes more than 99% of the iron from loaded holoferritin, recovering 70–80% of the original protein as monomeric apoferritin nanocages. Our work shows that pH conditions of the reduction step and the presence and nature of chelating agents affect the efficiency of iron removal. Furthermore, process conditions also seem to have an influence on the monomer:aggregate proportion present in the product. We also demonstrate that iron contents markedly increase ferritin absorbance at 280 nm. The influence of iron contents on absorbance at 280 nm precludes using this simple spectrophotometric measure for protein determination in ferritin-iron complexes. Apoferritin produced following our protocol only requires readily-available, cheap and biocompatible reagents, which makes this process standardizable, scalable and applicable to be used for *in vivo* applications of ferritin derivatives as well as nanotechnological and biotechnological uses.

1. Introduction

Ferritin is a natural iron–storage and iron–buffer protein, which can store up to 4500 iron atoms in the form of ferric oxyhydroxide mineral and releases iron in a controlled fashion. In humans, ferritin acts as a buffer against iron deficiency or iron overload [1]. Structurally, it presents a quaternary structure assembled by the interaction of twenty-four subunits that create a hollow sphere-like conformation with an outer diameter of 12 nm and a cavity of 8 nm [2], and two types of small channels formed between subunits – 3-fold symmetry and 4-fold symmetry channels – spanning from the outside into the internal cavity. In mammals, ferritin is formed by two kinds of subunits, light (L) and heavy (H) chains, which vary in proportion depending on the tissue source and function, adding up to a total protein molar mass of ~450 kDa. The H and L chains have different masses of 21 and 19 kDa, respectively. Each subunit has been assigned a specific role: H chains display ferroxidase activity able to catalyze the oxidation of Fe(II) to Fe (III) with molecular oxygen at body temperature, while L chains have nucleation sites for iron oxyhydroxides nucleation [3]. Fe(III) remains inside the protein cavity as insoluble precipitates and can be released from ferritin once it is reduced back to Fe(II) by external reducing agents.

Apoferritin is the iron-devoided spherical protein shell of ferritin that forms a biocompatible nanocage, which can be used to carry different encapsulated nanoparticles or functional molecules and is stable enough to be chemically or genetically modified to generate derivatives for nanotechnological and biotechnological applications. The synthesis of metallic nanoparticles inside apoferritin nanocages has been reported for gold [4], copper [5], silver [6] and platinum [7] among others, as well as alloys such gold-silver [8] and palladium-gold [9]. Some metal oxides have also been synthesized inside the ferritin cavity, such as Fe_3O_4 [10] and Co_3O_4 [11]. In addition, apoferritin has also been used to encapsulate molecules for drug delivery and biostabilization. Entrance of small molecules and ions into ferritin nanocages is

* Corresponding authors.
E-mail addresses: aolivera@ing.uchile.cl (Á. Olivera-Nappa), msoler@ing.uchile.cl (M. Soler).

https://doi.org/10.1016/j.jinorgbio.2017.11.019
Received 12 July 2017; Received in revised form 24 October 2017; Accepted 17 November 2017
Available online 21 November 2017
0162-0134/

believed to naturally occur through ferritin channels, but larger molecules have only been introduced into the cavity after pH-induced disassembly and reassembly of the apoferritin structure [12,13]. The incorporation of large organic molecules in apoferritin cavities for biomedical applications has been reported for gadolinium complexes with the natural anti-inflammatory molecule curcumin as a contrast agent for MRI [14] and for the chemotherapy molecule doxorubicin [15,16].

The main commercial apoferritin form is horse spleen apoferritin, available at a cost 3.5 times higher than iron-loaded holoferritin, probably due to the cost of iron removal and purification processes (Sigma-Aldrich, apoferritin Cat.# A3641, ferritin Cat.# F4503). There are several published methods to produce apoferritin from holoferritin. In general, these methods consist of 2 successive steps: first, a reduction of Fe(III) to Fe(II), and then removal of Fe(II) from the medium by exhaustive dialysis. In some methods, a chelator is added to aid iron removal.

In the Fe(III) reduction step, different reducing agents have been utilized: dithionite [17–20], $FMNH_2$ [19] and thioglycolic acid [19,21–26]. By far thioglycolic acid is the most used reductant in the literature to produce apoferritin. However, there is no consensus about the pH at which this reduction should be performed, since some authors use pH around 4 and others prefer neutral pH. The effects of pH on iron removal efficiency has been only partially studied [19], but no studies have been conducted to investigate protein structural changes with reduction treatments at different pH values.

The next step – the removal of Fe (II) ions from solution – has been performed mainly using exhaustive dialysis, aided in several publications with the addition of iron chelating agents such as 2,2′-bipyridyl, the most reported chelating molecule for apoferritin production [17,19,20,24,26–29], whereas other authors use dithionite or EDTA [22,30,31]. Iron reduction and remotion assisted by chaotropic agents such as urea have also been reported [32].

The iron content in ferritin (Fe/Ft), defined as the amount of iron atoms per protein nanocage, is the most important parameter for the generation of good quality iron-free apoferritin. However, there are two additional parameters that are key to determine the process efficiency: protein recovery and protein structural conformation at the end of the process. These three parameters should be considered to design a good protocol for apoferritin production.

In this work, we propose a method for efficient generation of iron-devoided ferritin in a single-day timeframe, using biocompatible non-denaturing reagents. For this aim, we compare the apoferritin formation process at acid and neutral conditions, testing different chelating agents. Using a set of complementary analytical techniques, we selected the best protocol to produce iron-free apoferritin nanocages based on lower ferritin iron content and higher protein recovery, while assessing protein conformation and size distribution.

2. Experimental

2.1. Chemicals

Horse spleen ferritin (HSF) was purchased from Sigma (F4503, Lot# SLBK7557V; 53 μg/μl ferritin in 150 mM NaCl). Thioglycolic acid (TGA) was purchased from Sigma. Ethylenediaminetetraacetic acid (EDTA) was purchased from Merck and 2,2′-bipyridyl (BiPy) from AK Scientific. Reagent grade ethanol was purchased from Merck. All solutions were prepared in deionized Milli Q water.

2.2. Apoferritin production

A volume of 125 μL of HFS solution (53 μg/μL) was incubated with 40 μL 10% TGA solution in 70 mM NaCl at two different pH (4.5 and 7), adding 200 μL of 1 M Bipy (dissolved in 50% ethanol) or 0.3 M EDTA, or an equivalent amount of solvent without chelating agent for control experiments. The mixture was incubated for 1 h at 4 °C, and then dialyzed using a membrane with a molecular cutoff (MWCO) of 14 kDa (Spectra/Por, Spectrumlabs) during 24 h against 70 mM NaCl at 4 °C, with two buffer changes (once every 8 h). Finally, the samples were centrifuged at 10,000 rpm for 1 h at 4 °C to remove denatured protein.

2.3. Protein characterization

Protein quantification was carried out using the bicinchoninic acid (BCA) method with ovalbumin as a reference [33]. Ferritin samples were subjected to size exclusion chromatography (SEC) using a FPLC Äkta Purifier 900 (GE Healthcare Life Sciences) with a GFC-1300 column (Supelco) for purification and detection at 280 nm (A_{280}). The size distribution of ferritin was measured by dynamic light scattering (DLS) using a Zetasizer (Malvern). The optical properties of the protein samples were measured using UV–vis spectroscopy with an AvaSpec-2048 (Avantes). BiPy titration of iron was performed by measuring absorbance at 520 nm of the BiPy-Fe complex and comparing with a calibration curve prepared with different amounts of Fe^{+3} (0–10 μg). Samples were prepared by adding HCl, TGA and BiPy. Absorbance was measured at 520 nm and Fe^{+3} calculated from the calibration curve. Iron quantification in ferritin and apoferritin samples was performed by inductively coupled plasma optical emission spectrometry (ICP-OES), carried out by the Unidad de Desarrollo Tecnológico from Universidad de Concepción, Coronel, Chile. Ferritin and apoferritin protein samples were analyzed in native 6% polyacrylamide electrophoresis gels (PAGE).

3. Results

3.1. Design of apoferritin production protocols

We designed six different experimental protocols to remove iron oxyhydroxides from horse spleen ferritin (HFS) in aqueous solution to obtain apoferritin. These protocols used two different pH conditions in the iron reduction step – pH 4.5 and pH 7 – and two chelating agents – 2,2′-bipyridyl (BiPy) and ethylenediaminetetraacetic acid (EDTA). We compared sample results with a control protocol with no chelating agent (NCh). The six experimental setups were performed in duplicate from the same initial sample and are summarized in Fig. 1.

3.2. UV–vis absorbance in ferritin samples and determination of iron content

The iron content of the starting material, HSF, and the apoferritin samples were studied by UV–vis spectroscopy and analyzed by ICP-OES. The UV–vis spectrum of the initial HSF depicted in both panels of Fig. 2, exhibits a broad absorption band from 300 to 550 nm attributed to iron oxides. This absorption band has been previously reported [18,34] and used to quantify iron oxides inside ferritin, with mean absorption at 420 nm. This UV–vis spectrum of HSF also shows two other absorption peaks, one at 280 nm, attributed in the literature to aromatic amino acids, and the other at 228 nm, attributed to the peptidic bond [33].

The UV–vis spectrum of the ferritin sample reduced with no chelator (NCh) at pH 4.5 (Fig. 2a) shows a decrease in the broad absorption peak between 300 and 550 nm compared with the HSF spectrum. Also, this spectrum displays reduced absorption peaks at 223 and 280 nm. The spectra of apoferritin samples reduced at pH 4.5 in the presence of chelating agents, both BiPy and EDTA, show a stronger reduction of the broad absorption band in the visible range and in both peaks in the UV band. It is evident from our results that peak intensities are affected by iron oxide contents in the sample. In addition, all iron-devoided protein samples show a blue shift of the peak attributed to peptidic bonds (200–220 nm), with the greatest shift exhibited by the BiPy sample. The spectra of the samples reduced at pH 7 (Fig. 2b) show the same pattern as their counterparts at pH 4.5, suggesting no optical difference

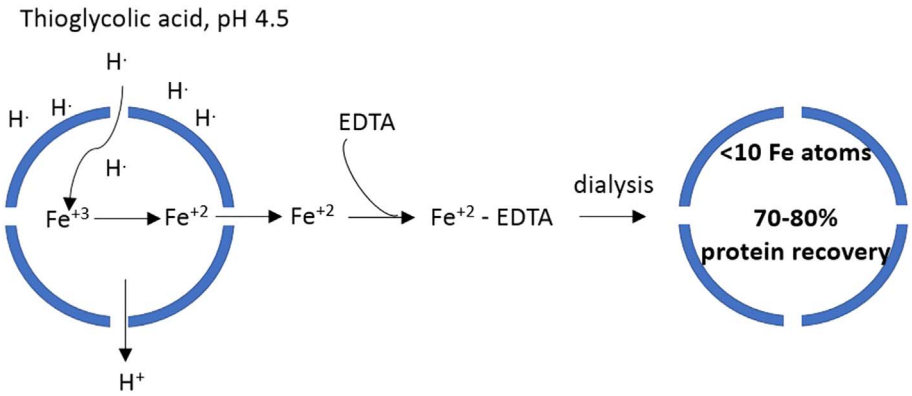

Fig. 1. Diagram of the proposed apoferritin formation protocols.

between treatments.

The iron content of the different samples was analyzed using BiPy Fe^{3+} titration and ICP-OES spectrometry. BiPy titration was used to measure iron(III) concentration in HSF and iron-devoided apoferritin samples with reference to a titration curve (Fig. S1). Results showed an average content of 1040 ± 283 iron atoms per ferritin nanocage in HSF, but the technique was inaccurate and not sensitive enough to detect iron in apoferritin samples.

The more sensitive ICP-OES spectrometry indicated that the initial iron-loaded HSF had an average of 818 ± 38 iron atoms per ferritin nanocage (Fe/Ft), if every ferritin molecule had the same iron content (Fig. 3). Fe/Ft ratio was then calculated for all the samples and compared with HSF (Fig. 3a for pH 4.5 and Fig. 3b for pH 7). Samples obtained with no chelating agents retained the highest amount of iron per protein nanocage, reflected by Fe/Ft ratios of 287 ± 7 with reduction at pH 4.5 and 543 ± 89 at pH 7, which represents a removal efficiency of 65% and 34% respectively (Fig. 3). Samples obtained by protocols using 2,2′-bipyridyl (BiPy) as a chelating agent improved iron removal, with Fe/Ft ratios of 111 ± 57 when reduced at pH 4.5 and 83 ± 1 at pH 7, representing a removal efficiency of 86% and 90% respectively. Finally, samples treated with EDTA retained the lowest amount of iron per ferritin nanocage, especially at pH 4.5, showing a Fe/Ft ratio of 5 ± 7 when reduced at pH 4.5 and 87 ± 40 at pH 7, with a removal efficiency of 99% and 89% respectively. Therefore, the comparison of the Fe/Ft ratio shows a significantly better removal of iron atoms at pH 4.5 for NCh and EDTA protocols, while there is no statistical difference at both pH values in the case of BiPy.

3.3. Apoferritin conformational characterization, size and recovery

HSF was analyzed by size exclusion chromatography (SEC) to study the initial holoferritin size and conformation features before following any apoferritin formation protocol. The chromatogram showed two protein elution peaks corresponding to the holoferritin sample (Fig. 4a), indicating the existence of at least two different ferritin species coexisting in the sample, previously noticed by other authors [27,35–39]. According to its lower molecular size, the second peak eluting at 5.8 mL can be attributed to monomeric ferritin, while the first protein peak at 4.4 mL, corresponds to species with larger molecular sizes than single ferritin 24-mer nanocages. This could indicate the presence of oligomeric or aggregated nanocage species. Protein concentration was determined for each HSF chromatographic peak, giving a monomer:aggregate proportion of 4:1.

The size distribution of HSF was characterized by dynamic light scattering (DLS). DLS analysis of the HSF ferritin sample before SEC indicates that ferritin nanocages have a size (hydrodynamic diameter, d_H) of 12 ± 1 nm (Fig. 5a), similar to the value previously reported by Jutz et al. [40]. Measurements of the collected fractions from the two different elutions after SEC show that the first elution peak (4.4 mL) has a d_H of 30 ± 2.2 nm, which would indicate the existence of ordered nanocage oligomers or ferritin aggregates. On the other hand, particle size measurements of the second elution peak fractions (5.8 mL) show a monodisperse d_H of 10 ± 1 nm, which is attributable to monomeric ferritin nanocages with a similar size to that of the HSF original sample. To further investigate the effect of surface charge on aggregation, we measured Z-potentials (ζ) of both elution peak fractions. The results

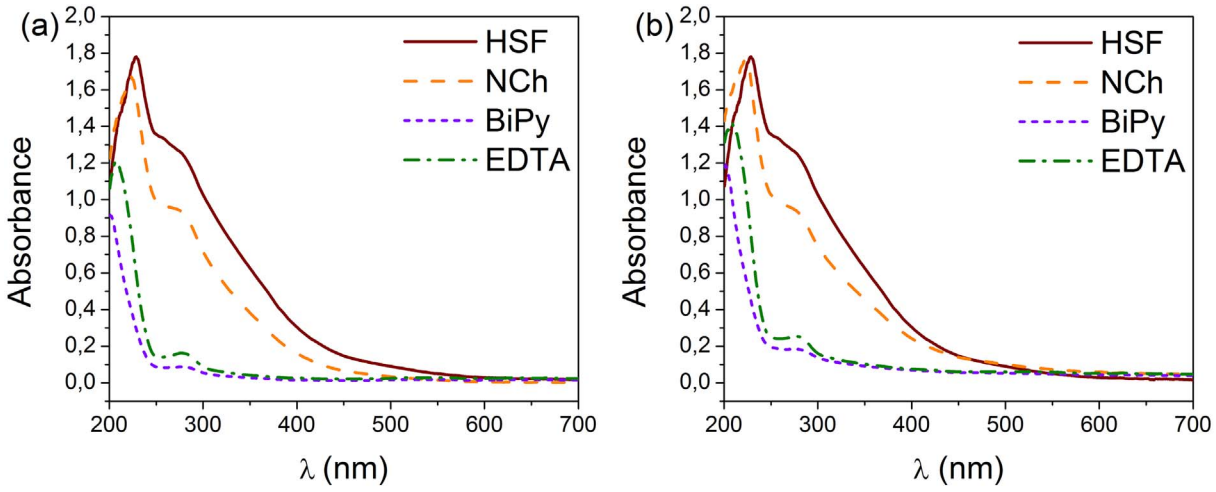

Fig. 2. UV–vis absorption spectra of apoferritin samples (NCh, BiPy and EDTA) reduced at pH 4.5 (a) and pH 7 (b) compared with the initial HSF ferritin sample.

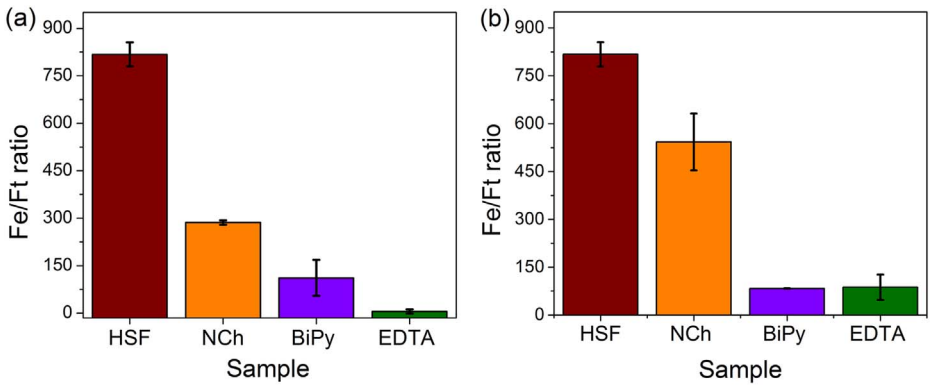

Fig. 3. Ratio of iron atoms per ferritin nanocage (Fe/Ft) from samples obtained following apoferritin protocols with different reduction conditions pH 4.5 (a) and pH 7 (b) compared to HSF.

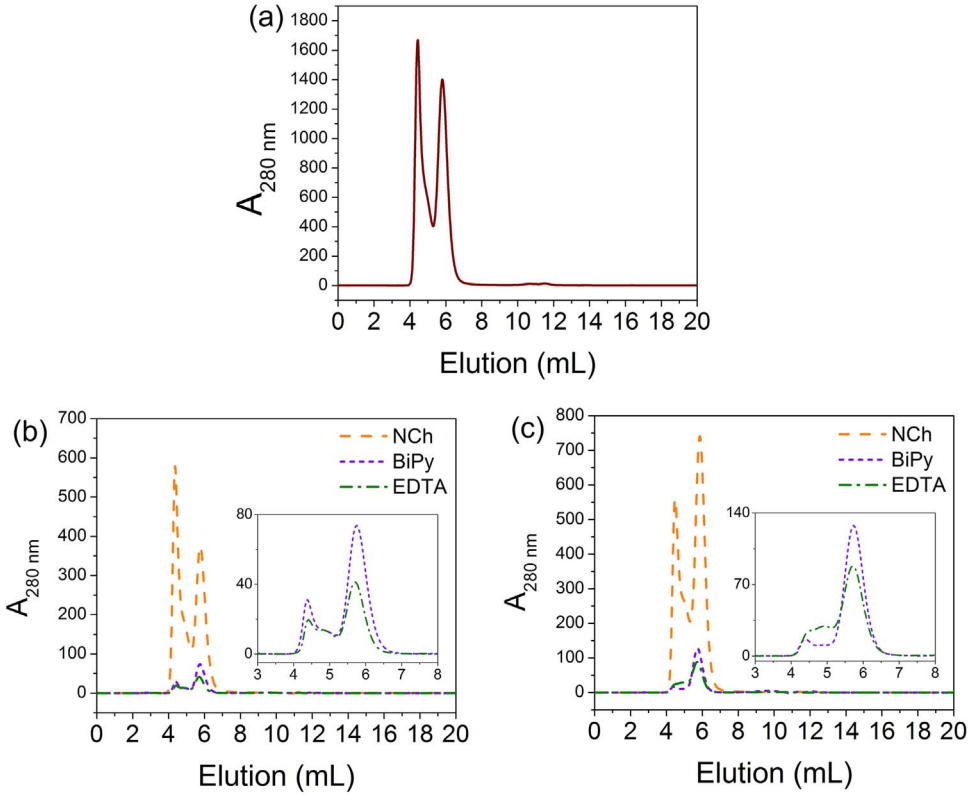

Fig. 4. Size exclusion chromatogram of commercial horse spleen ferritin (HSF) used as starting material (a), apoferritin produced at pH 4.5 (b) and pH 7 (c). Insets show a zoom of the chromatograms of samples obtained using protocols with chelating agents.

show that aggregated species have a ζ of −2.9 mV, while monomer species have a ζ of −12.6 mV. Finally, the comparison of Fe/Ft ratio of monomeric and aggregated fractions, 1072 ± 410 and 2730 ± 198 respectively, shows that iron content varies depending on the oligomeric state of ferritin, being higher for ferritin oligomers or aggregates.

Apoferritin samples were analyzed by native PAGE (Fig. S2), SEC (Fig. 4b–c) and DLS to determine the existence of monomeric and aggregated species. Native gel electrophoresis results indicate that there is no relevant difference between the original iron-loaded HSF and treated apoferritin samples, both in abundance and in migration pattern of bands. Chromatograms of NCh samples showed two protein elution peaks with a predominant aggregate peak, when reduced at pH 4.5 (Fig. 4b), resembling the original HSF sample (Fig. 4a). NCh samples reduced at pH 7 (Fig. 4c) showed a larger proportion of the monomeric ferritin peak. The use of chelating agents (BiPy and EDTA) tends to further reduce the height of the protein aggregate peak, with more relative impact when the reduction step is performed at pH 7. For all samples, no peaks were observed at higher elution volumes that could be attributed to ferritin fragments.

The size distribution of apoferritin samples is shown in Fig. 5b–c. The hydrodynamic diameter in all samples is on average 11 ± 1 nm. A small trend toward lower sizes was observed in BiPy-treated samples. In the case of NCh samples, the hydrodynamic diameter in samples treated at pH 4.5 is markedly larger than the average. However, no statistically significant size differences were detected in comparison to HSF at any treatment condition.

Finally, we estimated protein recovery in each sample based on the initial amount of HSF (Table 1). NCh samples showed the maximum recovery yield of 70–80%, independently of the pH of the reduction process. With EDTA at pH 4.5 and 7, protein recovery yields were 72% and 78%, respectively, which are not significantly different from those without chelators. However, protein recovery significantly drops down to ~40% when BiPy is used as a chelating agent. For all treatments, acid pH does not cause protein loss by denaturation.

4. Discussion

Apoferritin is a highly valuable material for nanotechnology applications, since it provides a confined cavity surrounded by a protein shell suitable for monodisperse nanoparticle synthesis or for encapsulation of

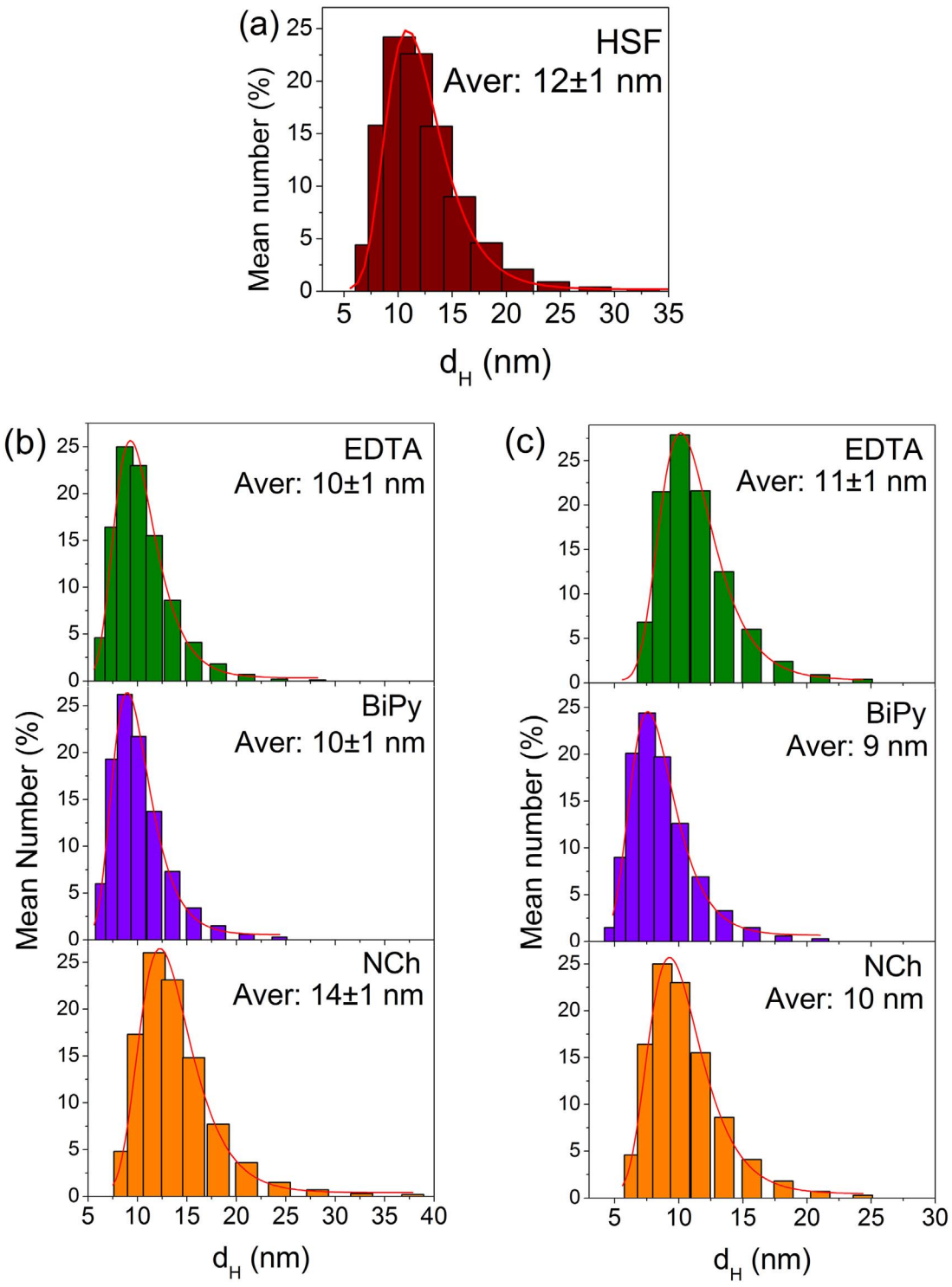

Fig. 5. Size distribution graphs of commercial horse spleen ferritin (HSF) used as starting material (a) and samples obtained after apoferritin formation protocols with reduction steps performed at pH 4.5 (b) and at pH 7 (c).

Table 1
Protein recovery yield.

Sample	Protein recovery (%)		
	NCh	BiPy	EDTA
pH 4.5	73 ± 18	36 ± 7	72 ± 3
pH 7	76 ± 12	42 ± 8	78 ± 3

different target molecules. Apoferritin is produced from holoferritin usually by a 2-step process that involves iron reduction followed by iron removal. Several protocols have been published for apoferritin production, using different iron reductants, pH conditions during reduction and, in some cases, chelating agents. These previous studies have focused their results in iron removal efficiency, without considering protein yield and conformational state. For these reasons, we tested six different protocols to produce apoferritin and analyzed their iron content, protein conformational state, size and protein yield.

4.1. Influence of iron content on ferritin UV–vis absorbance

UV–vis spectroscopy can detect large differences in iron content between samples (Fig. 2), but not more subtle differences. Our results showed that ferritin UV–vis spectra has a wide and relatively weak absorbance band around 420 nm and a strong absorbance peak at 280 nm, dependent on the presence of iron oxyhydroxides in the protein cavity. In particular, we have shown a relative decrease in the absorbance band at 280 nm (A_{280}) as function of the iron content (Figs. 2 and 4b–c). Gálvez et al. [26] described that iron oxyhydroxides in the protein cavity have different crystalline structures corresponding to magnetite (Fe_3O_4), ferrihydrite (FeOOH) and hematite (Fe_2O_3), which abundances depend on the Fe/Ft ratio. Additionally, other studies have shown that each iron oxide has different optical properties and absorption features in the UV range [41–44]. Therefore, we attributed A_{280} intensity changes mostly to the content and type of iron oxide, and not only to aromatic amino acid absorption. This same phenomenon has also been reported for other iron containing proteins, such as transferrins [45]. The calculated molar absorptivity coefficient at 280 nm (ε^{280}) for HSF was 1,552,000 $M^{-1}\,cm^{-1}$, whereas the ε^{280} of apoferritin with ~10 Fe/Ft was 411,000 $M^{-1}\,cm^{-1}$, close to the 468,000 $M^{-1}\,cm^{-1}$ value reported by Gálvez et al. [26]. This shows that the presence of iron oxyhydroxides inside the protein cavity contributes to A_{280} in a non-linear manner. According to this, the widely used protein determination method measuring A_{280} is not reliable for holoferritin or apoferritin quantification, since ε^{280} changes according to ferritin iron content. For the same reason, a direct comparison of A_{280} peak height in SEC to determine relative abundances of monomeric and aggregate ferritin forms in a sample cannot be done due to the presence of varying iron loads.

4.2. Iron removal efficiency

Iron removal efficiencies were studied by comparing the Fe/Ft ratios, from ICP-EOS and BCA results, to determine the effect of pH and chelating agent. Contrasting different pH conditions, our results demonstrated that reduction at pH 4.5 showed the highest iron removal efficiency from ferritin. This can be explained by the fact that reduction of Fe^{3+} to Fe^{2+} consumes H^+ in aqueous media. Therefore, at higher pH the number of protons available to carry out this reduction limits the amount of Fe^{2+} formed for subsequent removal. On the other hand, the use of chelating agents increases the amount of iron removed from holoferritin. This is explained by the high binding affinity of Fe^{2+} ions to chelating agents, such as BiPy or EDTA, which prevents iron recapture into the protein nanocage. Furthermore, we observed a combined effect of the pH and chelating agents on iron removal efficiency.

The best result was obtained when iron was reduced at pH 4.5 and EDTA was used as a chelator. The formation constant of the most stable 1:1 $[Fe(EDTA)]^{2-}$ complex has a value of 6×10^6 at pH 4.5 and 8×10^{10} at pH 7.0 [46], which makes EDTA a better chelating agent at neutral pH. The pK_a constant of the $EDTA^{2-}$ species required for iron chelation is 2.7, which means that more than 99% of all $EDTA^{2-}$ molecules are available to form complexes with iron at pH 4.5 or higher. Since EDTA-assisted iron removal is better at pH 4.5, Fe^{2+} removal efficiency should be limited by the pH-dependent iron reduction step and not by the complex formation equilibrium.

Both EDTA and BiPy remove essentially the same amount of iron from HSF at pH 7.0. At this pH the most stable 3:1 $[Fe(BiPy)_3]^{2+}$ complex has a formation constant of 2×10^9 [47], which is similar to the formation constant of the stable Fe-EDTA complex. This shows that complexation is not the limiting step at pH 7.0, as previously demonstrated for EDTA. However, apoferritin samples produced with BiPy at neutral pH show a significantly higher iron content than those treated at acidic pH, contrary to EDTA-treated samples. This can be explained considering that BiPy groups have a pK_a of 4.3 and consequently tend to be ~50% protonated at pH 4.5. Since both pyridyl groups must be deprotonated to chelate Fe^{2+}, the effectiveness of BiPy as a chelating agent is approximately half reduced at pH 4.5. Thus, contrary to the EDTA case, complexation and not reduction is the limiting step at pH 4.5 for BiPy-assisted iron removal from ferritin. Therefore, since reduction is favoured by an acidic pH value as previously discussed and only EDTA is able to chelate Fe^{2+} at lower pH conditions, then EDTA should be the preferred chelating agent to remove the largest amount of iron from ferritin, as demonstrated by our results.

4.3. Size and conformation analysis

We have shown that in all our samples ferritin is present as nanocage monomers and aggregates, which elute in separate SEC peaks. This was confirmed by collecting HSF elution peaks in different fractions and measuring particle size distribution and protein concentration. In HSF, monomers are roughly 80% of the total protein. For apoferritin samples, we observed peaks eluting at the same volumes, which suggest apoferritin has similar monomer and aggregate forms. We measured the size distribution of the apoferritin sample and that was not statistically different from the size distribution of the monomeric untreated HSF fraction, which indicates that apoferritin is mainly in a monomeric form. This further confirms that the iron removal process tends to retain the size of the initial protein and do not affect its quaternary structure.

Based on measured Z-potential (ζ) values, monomers have a higher surface charge than aggregates, suggesting that the total charge in aggregates has been somewhat compensated. Aggregate formation can be attributed to electrostatic and chemical interactions between protein surfaces, where the exposed groups locally decrease the repulsion between proteins [38,39], either by coulombic attraction, hydrogen bonding, hydrophobic interaction or generation of disulfide bridges [35]. Considering that iron oxyhydroxide content is higher in aggregates, charge compensation could be related to higher iron load, but this remains to be further investigated. Furthermore, independently of ferritin iron content, whether aggregation itself causes charge neutralization or aggregation occurs due to charge compensation also remains a question to be answered.

In relation to the influence of reduction pH conditions, higher aggregate peak areas were observed in samples reduced at pH 4.5 compared with treatments at pH 7 (Fig. 4). This can be related to aggregate formation due to exposure of ferritin to pH conditions close to its isoelectric point (pI ~ 4.5) [48], which could generate low electrostatic repulsion between nanocages. Once nanocage aggregates are formed, other kind of interactions can stabilise this configuration. Consistently, Niitsu and Listowsky [35] had reported that the reduction of the iron core at acid pH and subsequent removal of iron ions by a chelating agent, did not eliminate the formation of ferritin aggregates. In support of this explanation, we observed that apoferritin samples produced with chelators at pH 7 exhibit predominantly the monomer state. This can be explained by the findings of Crichton and Bryce [36], who showed partial disaggregation of aggregates at higher pH values.

4.4. Protein yield

Protein recovery is a key parameter scarcely reported in apoferritin formation protocols. The work from Wong et al. [25] informed a protein recovery of 65 to 80% when apoferritin formation was performed by TGA reduction and exhaustive dialysis, which is similar to our results. Our findings indicate that apoferritin formation process by TGA reduction and dialysis alone (NCh protocol samples) induce a protein loss of 20–30%. Moreover, we observed that the use of BiPy as chelating agent is detrimental for protein recovery (36–42% yield) as shown in Table 1, but EDTA protocols show much higher protein recovery yields (72–78%).

5. Conclusion

We presented a very effective protocol to remove almost all iron atoms from the ferritin cavity maintaining the protein quaternary conformation, including the presence of monomeric and multimeric forms, and with a high overall protein recovery.

The high removal efficiency depends both on the pH used for the reduction step and the nature of the chelating agent. Our results demonstrated that removal is more favourable at low pH, independently of the chelating agent. We also observed that the presence of chelating agents helps to remove Fe^{2+} from ferritin. BiPy and EDTA have comparable performances at neutral pH, but EDTA has a greater effect at low pH. Therefore, our most efficient method uses pH 4.5 in the reduction step and EDTA as a chelating agent and allowed us to remove up to 99% of iron from ferritin with 70–80% protein recovery.

Additionally, we have demonstrated that UV–vis absorption is not a good method to quantify protein in ferritin samples, including protein quantification in chromatographic peaks. Absorption at 280 nm is non-linearly related to both protein amount and iron content inside the ferritin cavity. These results support the use of more sensitive and specific analytical techniques such as those used in this study to determine the content of iron atoms per ferritin nanocage, especially in low iron content samples.

Apoferritin produced in this way is ready to be used in demanding nanotechnological applications due to its very low iron load and conformational integrity. The proposed process requires readily-available, cheap and biocompatible reagents, which makes this process standardizable, scalable and suitable to be used for biotechnological and *in vivo* uses of ferritin derivatives.

Acknowledgments

The authors acknowledge the funding of Project U-Redes (UR-003/2015) “FERRITEAM: design and applications of ferritin-based bionanomaterials” from University of Chile. The authors would like to thank FONDECYT grants 1141311 and 1161775 from CONICYT for funding and support for their work. IM would like to thank CONICYT for his Doctorate Scholarship. M. Santiago and AO-N would like to acknowledge the funding of Project PIA FB0001 from CONICYT (Center of Biotechnology and Bioengineering, CeBiB). The authors declare no competing financial interest.

Appendix A. Supplementary data

Supplementary data to this article can be found online at https://doi.org/10.1016/j.jinorgbio.2017.11.019.

References

[1] A. Jacobs, F. Miller, M. Worwood, M. Beamish, C. Wardrop, Br. Med. J. 4 (1972) 206–208.
[2] M. Uchida, S. Kang, C. Reichhardt, K. Harlen, T. Douglas, Biochim. Biophys. Acta 1800 (2010) 834–845.
[3] D. He, J. Marles-Wright, New Biotechnol. 32 (2015) 651–657.
[4] R. Fan, S.W. Chew, V.V. Cheong, B.P. Orner, Small 6 (2010) 1483–1487.
[5] N. Gálvez, B. Fernandez, E. Valero, P. Sánchez, R. Cuesta, J.M. Domínguez-Vera, C. R. Chim. 11 (2008) 1207–1212.
[6] O. Kasyutich, A. Ilari, A. Fiorillo, D. Tatchev, A. Hoell, P. Ceci, J. Am. Chem. Soc. 132 (2010) 3621–3627.
[7] Q. Deng, B. Yang, J. Wang, C. Whiteley, X. Wang, Biotechnol. Lett. 31 (2009) 1505–1509.
[8] Y. Shin, A. Dohnalkova, Y. Lin, J. Phys. Chem. C 114 (2010) 5985–5989.
[9] M. Suzuki, M. Abe, T. Ueno, S. Abe, T. Goto, Y. Toda, T. Akita, Y. Yamada, Y. Watanabe, Chem. Commun. (2009) 4871–4873.
[10] M. Uchida, M. Terashima, C.H. Cunningham, Y. Suzuki, D.A. Willits, A.F. Willis, P.C. Yang, P.S. Tsao, M.V. McConnell, M.J. Young, Magn. Reson. Med. 60 (2008) 1073–1081.
[11] R. Tsukamoto, K. Iwahori, M. Muraoka, I. Yamashita, Bull. Chem. Soc. Jpn. 78 (2005) 2075–2081.
[12] M. Kim, Y. Rho, K.S. Jin, B. Ahn, S. Jung, H. Kim, M. Ree, Biomacromolecules 12 (2011) 1629–1640.
[13] H. Chen, S. Zhang, C. Xu, G. Zhao, Chem. Commun. 52 (2016) 7402–7405.
[14] J.C. Cutrin, S.G. Crich, D. Burghelea, W. Dastru, S. Aime, Mol. Pharm. 10 (2013) 2079–2085.
[15] M.A. Kilic, E. Ozlu, S. Calis, J. Biomed. Nanotechnol. 8 (2012) 508–514.
[16] K. Tmejova, D. Hynek, P. Kopel, S. Dostalova, K. Smerkova, M. Stanisavljevic, H.V. Nguyen, L. Nejdl, M. Vaculovicova, S. Krizkova, R. Kizek, V. Adam, Int. J. Electrochem. Sci. 8 (2013) 12658–12671.
[17] S. Granick, L. Michaelis, J. Biol. Chem. 147 (1943) 91–97.
[18] I.G. Macara, T.G. Hoy, P.M. Harrison, Biochem. J. 126 (1972) 151–162.
[19] F. Funk, J.-P. Lenders, R.R. Crichton, W. Schneider, Eur. J. Biochem. 152 (1985) 167–172.
[20] G. Zhao, F. Bou-Abdallah, P. Arosio, S. Levi, C. Janus-Chandler, N.D. Chasteen, Biochemistry 42 (2003) 3142–3150.
[21] A. Treffry, P.M. Harrison, Biochem. J. 171 (1978) 313–320.
[22] M. Gerl, R. Jaenicke, Eur. Biophys. J. 15 (1987) 103–109.
[23] M.-S. Joo, G. Tourillon, D. Sayers, E. Theil, Biol. Met. 3 (1990) 171–175.
[24] S. Cavallo, G. Mei, S. Stefanini, N. Rosato, A. Finazzi-Agró, E. Chiancone, Protein Sci. 7 (1998) 427–432.
[25] K.K.W. Wong, T. Douglas, S. Gider, D.D. Awschalom, S. Mann, Chemistry of Materials, vol. 10, American Chemical Society, 1998, pp. 279–285.
[26] N. Gálvez, B. Fernández, P. Sánchez, R. Cuesta, M. Ceolín, M. Clemente-Leon, S. Trasobares, M. López-Haro, J.J. Calvino, O. Stéphan, J.M. Dominguez-Vera, J. Am. Chem. Soc. 130 (2008) 8062–8068.
[27] S.S. Lee, G.W. Richter, Biochemistry 15 (1976) 65–70.
[28] S. Levi, S. Yewdall, P. Harrison, P. Santambrogio, A. Cozzi, E. Rovida, A. Albertini, P. Arosio, Biochem. J. 288 (1992) 591–596.
[29] M. Clemente-Leon, E. Coronado, A. Soriano-Portillo, E. Colacio, J.M. Domínguez-Vera, N. Gálvez, R. Madueño, M.T. Martín-Romero, Langmuir 22 (2006) 6993–7000.
[30] S. Kim, J.-H. Lee, J.H. Seok, Y.-H. Park, S.W. Jung, A.E. Cho, C. Lee, M.S. Chung, K.H. Kim, J. Mol. Biol. 428 (2016) 5007–5018.
[31] S. Stefanini, E. Chiancone, P. Vecchini, E. Antonini, Mol. Cell. Biochem. 13 (1976) 55–61.
[32] N. Galvez, B. Ruiz, R. Cuesta, E. Colacio, J.M. Dominguez-Vera, Inorg. Chem. 44 (2005) 2706–2709.
[33] J.M. Walker, The Protein Protocols Handbook, Humana Press, Totowa, 2002.
[34] J.C. Salgado, A. Olivera-Nappa, Z.P. Gerdtzen, V. Tapia, E.C. Theil, C. Conca, M.T. Nunez, BMC Syst. Biol. 4 (2010) 147.
[35] Y. Niitsu, I. Listowsky, Biochemistry 12 (1973) 4690–4695.
[36] R.R. Crichton, C.F. Bryce, Biochem. J. 133 (1973) 289–299.
[37] M. Williams, P.M. Harrison, Biochem. J. 110 (1968) 265–280.
[38] D.N. Petsev, B.R. Thomas, S.-T. Yau, P.G. Vekilov, Biophys. J. 78 (2000) 2060–2069.
[39] D.N. Petsev, B.R. Thomas, S.-T. Yau, D. Tsekova, C. Nanev, W.W. Wilson, P.G. Vekilov, J. Cryst. Growth 232 (2001) 21–29.
[40] G. Jutz, P. van Rijn, B. Santos Miranda, A. Boker, Chem. Rev. 115 (2015) 1653–1701.
[41] M. Chirita, I. Grozescu, L. Taubert, H. Radulescu, E. Princz, É. Stefanovits-Bányai, C. Caramalau, L. Bulgariu, M. Macoveanu, C. Muntean, Chem. Bull. 54 (2009) 1–8.
[42] P. Mallick, B. Dash, Nanosci. Nanotechnol. 3 (2013) 130–134.
[43] K. Tharani, L.C. Nehri, Int. J. Adv. Res. Phys. Sci. 2 (2015) 47–50.
[44] A. Kaushik, R. Khan, P.R. Solanki, P. Pandey, J. Alam, S. Ahmad, B. Malhotra, Biosens. Bioelectron. 24 (2008) 676–683.
[45] N.G. James, S.L. Byrne, A.N. Steere, V.C. Smith, R.T. MacGillivray, A.B. Mason, Biochemistry 48 (2009) 2858–2867.
[46] D.C. Harris, Quantitative Chemical Analysis, W. H. Freeman, New York, 2006.
[47] P. Atkins, T. Overton, J. Rourke, M. Weller, F. Armstrong, M. Hagerman, Inorganic Chemistry, Oxford University Press, Oxford, 2009.
[48] P.M. Harrison, Biochem. Educ. 14 (1986) 154–162.